

Fig. 1: Comparisons of deraining methods working on LFIs. The de-rained central sub-view generated by each method is scored with the PSNR/SSIM. The best value is highlighted with **bold**, and the second-best value is colored with **cyan**.



Fig. 2: Comparisons of deraining methods working on LFIs. The de-rained central sub-view generated by each method is scored with the PSNR/SSIM. The best value is highlighted with **bold**, and the second-best value is colored with **cyan**.

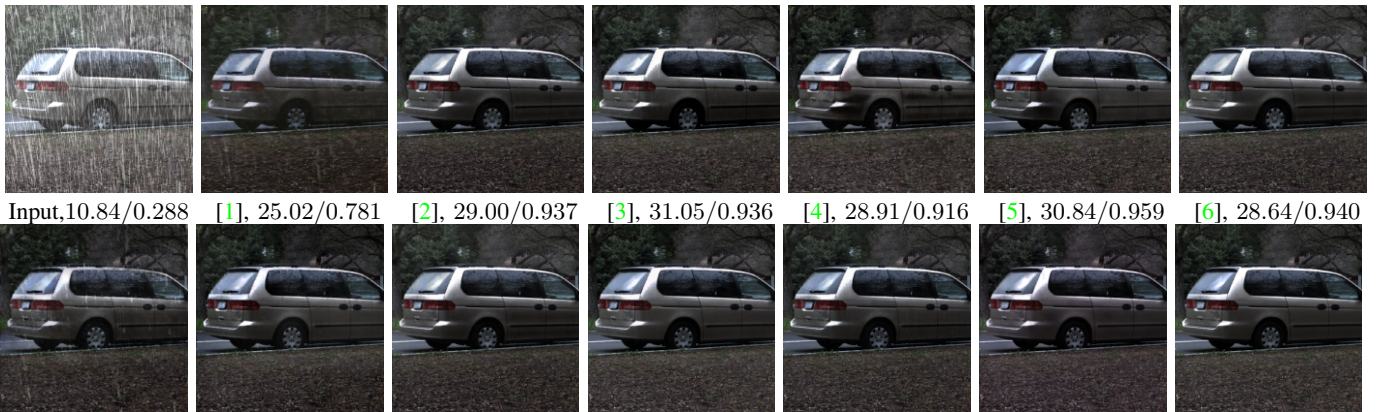


Fig. 3: Comparisons of deraining methods working on LFIs. The de-rained central sub-view generated by each method is scored with the PSNR/SSIM. The best value is highlighted with **bold**, and the second-best value is colored with **cyan**.



Fig. 4: Comparisons of deraining methods working on LFIs. The de-rained central sub-view generated by each method is scored with the PSNR/SSIM. The best value is highlighted with **bold**, and the second-best value is colored with **cyan**.

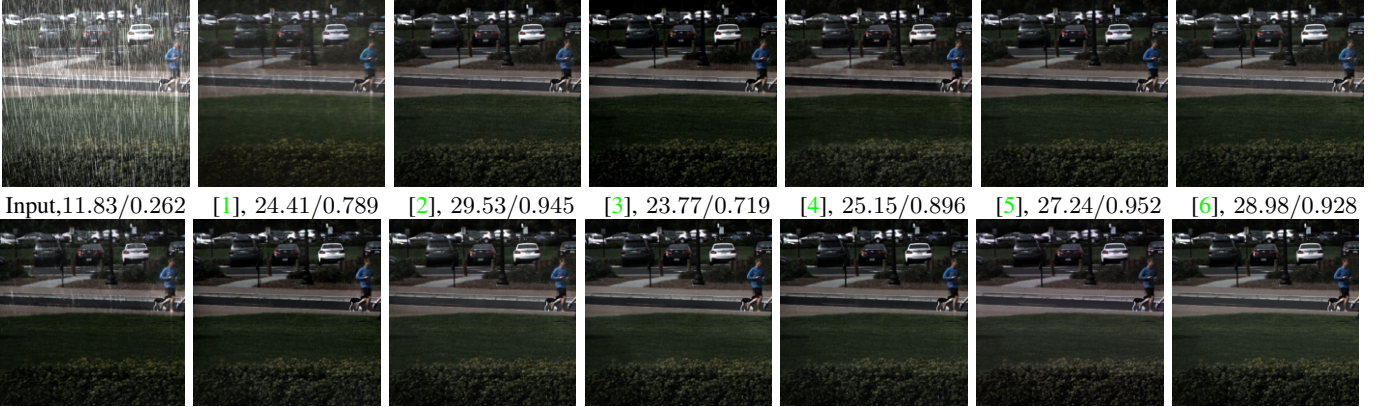


Fig. 5: Comparisons of deraining methods working on synthetic LFIs. The de-rained central sub-view generated by each method is scored with the PSNR/SSIM. The best value is highlighted with **bold**, and the second-best value is colored with **cyan**.

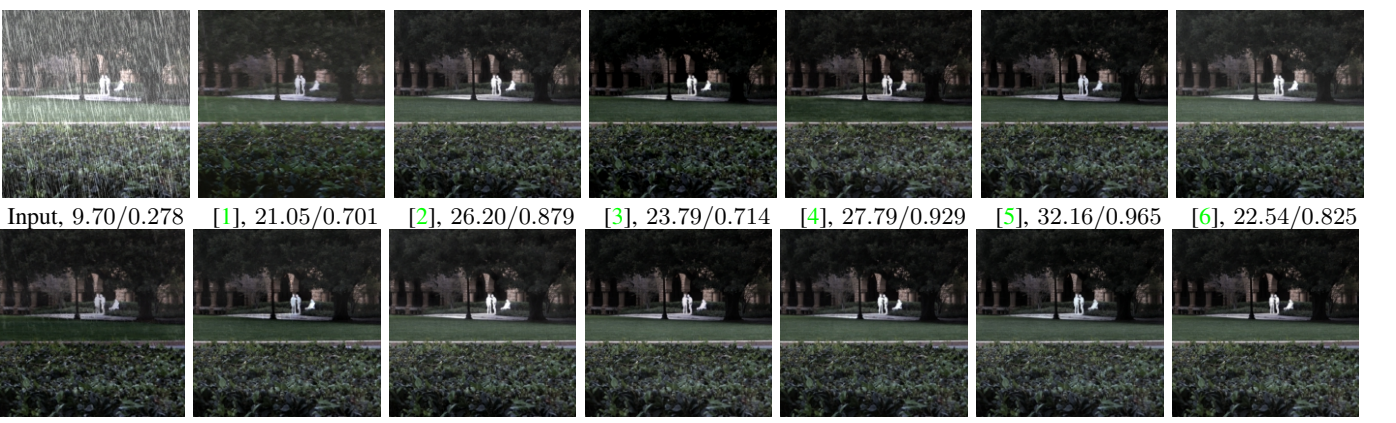


Fig. 6: Comparisons of deraining methods working on synthetic LFIs. The de-rained central sub-view generated by each method is scored with the PSNR/SSIM. The best value is highlighted with **bold**, and the second-best value is colored with **cyan**.



Fig. 7: Comparisons of deraining methods working on synthetic LFIs. The de-rained central sub-view generated by each method is scored with the PSNR/SSIM. The best value is highlighted with **bold**, and the second-best value is colored with **cyan**.

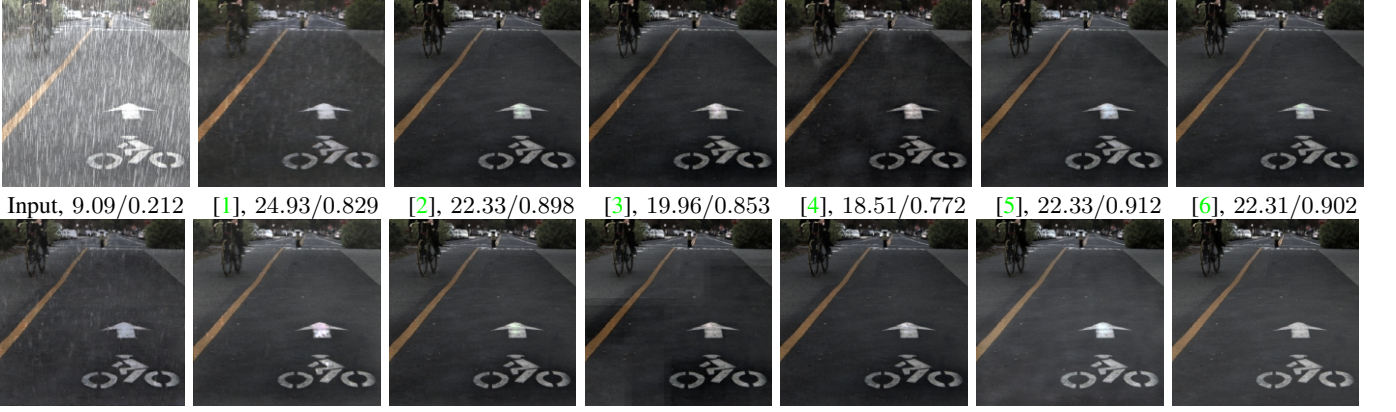


Fig. 8: Comparisons of deraining methods working on synthetic LFIs. The de-rained central sub-view generated by each method is scored with the PSNR/SSIM. The best value is highlighted with **bold**, and the second-best value is colored with **cyan**.

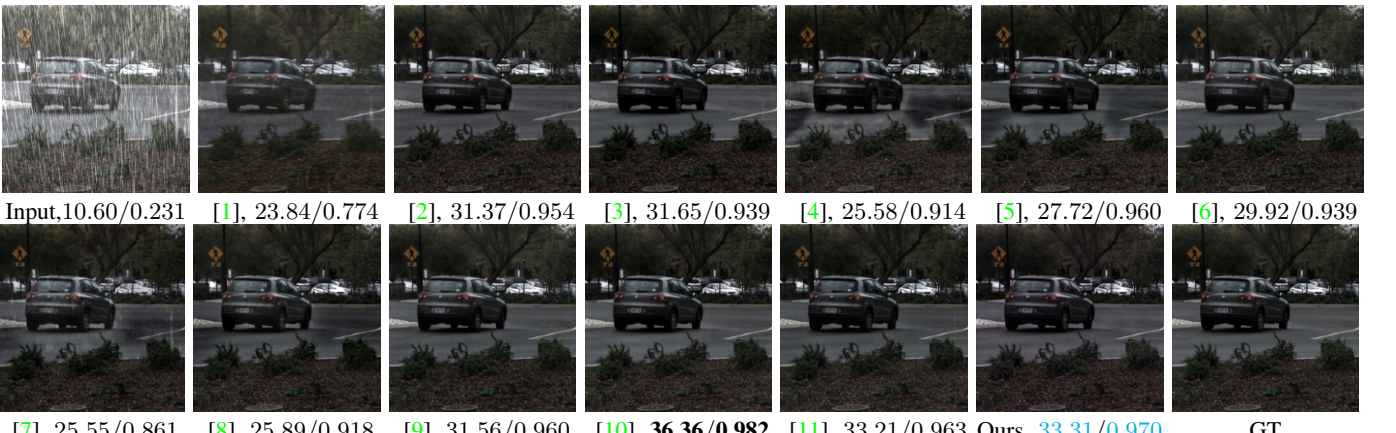


Fig. 9: Comparisons of deraining methods working on synthetic LFIs. The de-rained central sub-view generated by each method is scored with the PSNR/SSIM. The best value is highlighted with **bold**, and the second-best value is colored with **cyan**.



Fig. 10: Comparisons of deraining methods working on synthetic LFIs. The de-rained central sub-view generated by each method is scored with the PSNR/SSIM. The best value is highlighted with **bold**, and the second-best value is colored with cyan.



Fig. 11: Comparisons of deraining methods working on synthetic LFIs. The de-rained central sub-view generated by each method is scored with the PSNR/SSIM. The best value is highlighted with **bold**, and the second-best value is colored with cyan.



Fig. 12: Comparisons of deraining methods working on synthetic LFIs. The de-rained central sub-view generated by each method is scored with the PSNR/SSIM. The best value is highlighted with **bold**, and the second-best value is colored with cyan.

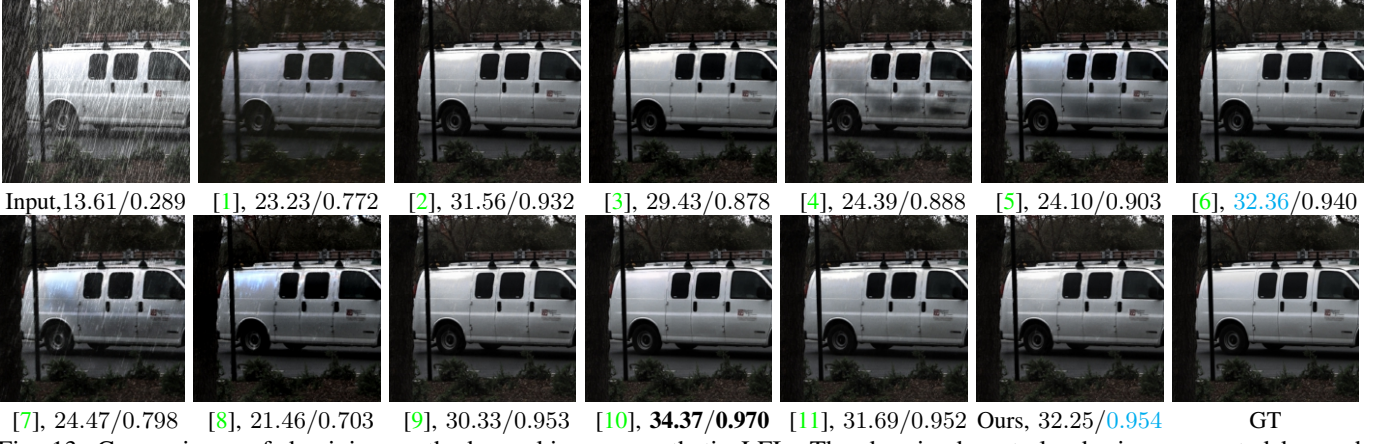


Fig. 13: Comparisons of deraining methods working on synthetic LFIs. The de-rained central sub-view generated by each method is scored with the PSNR/SSIM. The best value is highlighted with **bold**, and the second-best value is colored with cyan.



Fig. 14: Comparisons of deraining methods working on synthetic LFIs. The de-rained central sub-view generated by each method is scored with the PSNR/SSIM. The best value is highlighted with **bold**, and the second-best value is colored with cyan.



Fig. 15: Comparisons of deraining methods working on synthetic LFIs. The de-rained central sub-view generated by each method is scored with the PSNR/SSIM. The best value is highlighted with **bold**, and the second-best value is colored with cyan.



Fig. 16: Comparisons of deraining methods working on synthetic LFIs. The de-rained central sub-view generated by each method is scored with the PSNR/SSIM. The best value is highlighted with **bold**, and the second-best value is colored with cyan.



Fig. 17: Comparisons of deraining methods working on synthetic LFIs. The de-rained central sub-view generated by each method is scored with the PSNR/SSIM. The best value is highlighted with **bold**, and the second-best value is colored with cyan.



Fig. 18: Comparisons of deraining methods working on synthetic LFIs. The de-rained central sub-view generated by each method is scored with the PSNR/SSIM. The best value is highlighted with **bold**, and the second-best value is colored with cyan.



Fig. 19: Comparisons of deraining methods working on synthetic LFIs. The de-rained central sub-view generated by each method is scored with the PSNR/SSIM. The best value is highlighted with **bold**, and the second-best value is colored with cyan.

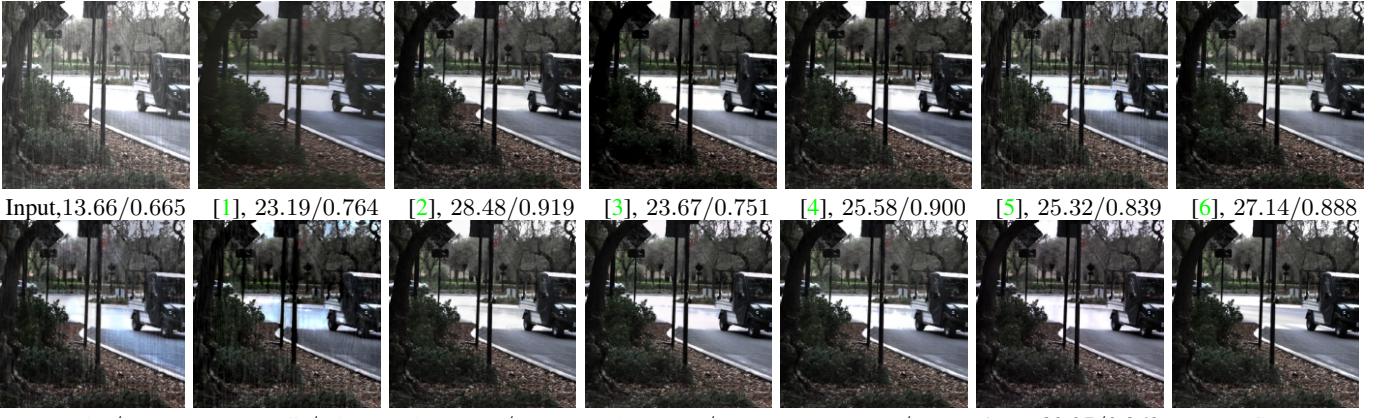


Fig. 20: Comparisons of deraining methods working on synthetic LFIs. The de-rained central sub-view generated by each method is scored with the PSNR/SSIM. The best value is highlighted with **bold**, and the second-best value is colored with cyan.



Fig. 21: Comparison of deraining methods on synthetic LFIs. The de-rained center sub-view generated by each method is evaluated on PSNR/SSIM. The best value is highlighted in **bold**, and the second-best value is colored in cyan.



Fig. 22: Comparison of deraining methods on synthetic LFIs. The de-rained center sub-view generated by each method is evaluated on PSNR/SSIM. The best value is highlighted in **bold**, and the second-best value is colored in **cyan**.



Fig. 23: Comparison of deraining methods on synthetic LFIs. The de-rained center sub-view generated by each method is evaluated on PSNR/SSIM. The best value is highlighted in **bold**, and the second-best value is colored in **cyan**.

REFERENCES

- [1] R. Li, L. Cheong, and R. T. Tan, “Heavy rain image restoration: Integrating physics model and conditional adversarial learning,” in *Proc. IEEE CVPR*, pp. 1633–1642, 2019.
- [2] W. Wei, D. Meng, Q. Zhao, Z. Xu, and Y. Wu, “Semi-supervised transfer learning for image rain removal,” in *Proc. IEEE CVPR*, pp. 3877–3886, 2019.
- [3] K. Jiang, Z. Wang, P. Yi, C. Chen, Z. Han, T. Lu, B. Huang, and J. Jiang, “Decomposition makes better rain removal: An improved attention-guided deraining network,” *IEEE TCSVT*, 2020.
- [4] W. Yang, R. T. Tan, J. Feng, Z. Guo, S. Yan, and J. Liu, “Joint rain detection and removal from a single image with contextualized deep networks,” *IEEE TPAMI*, vol. 42, no. 6, pp. 1377–1393, 2020.
- [5] D. Ren, W. Shang, P. Zhu, Q. Hu, D. Meng, and W. Zuo, “Single image deraining using bilateral recurrent network,” *IEEE TIP*, vol. 29, pp. 6852–6863, 2020.
- [6] R. Yasarla, V. A. Sindagi, and V. M. Patel, “Syn2real transfer learning for image deraining using gaussian processes,” in *Proc. CVPR*, pp. 2726–2736, 2020.
- [7] S. W. Zamir, A. Arora, S. Khan, M. Hayat, F. S. Khan, M.-H. Yang, and L. Shao, “Multi-stage progressive image restoration,” in *Proc. IEEE/CVF CVPR*, pp. 14821–14831, 2021.
- [8] X. Hu, L. Zhu, T. Wang, C.-W. Fu, and P.-A. Heng, “Single-image real-time rain removal based on depth-guided non-local features,” *IEEE TIP*, vol. 30, pp. 1759–1770, 2021.
- [9] Y. Ding, M. Li, T. Yan, F. Zhang, Y. Liu, and R. W. Lau, “Rain streak removal from light field images,” *IEEE TCSVT*, pp. 1–1, 2021.
- [10] J. Xiao, X. Fu, A. Liu, F. Wu, and Z.-J. Zha, “Image de-raining transformer,” *IEEE TPAMI*, 2022.
- [11] S. W. Zamir, A. Arora, S. Khan, M. Hayat, F. S. Khan, and M.-H. Yang, “Restormer: Efficient transformer for high-resolution image restoration,” in *Proc. IEEE/CVF CVPR*, pp. 5728–5739, 2022.
- [12] T. Wang, X. Yang, K. Xu, S. Chen, Q. Zhang, and R. W. Lau, “Spatial attentive single-image deraining with a high quality real rain dataset,” in *Proc. IEEE CVPR*, pp. 12270–12279, 2019.
- [13] K. Jiang, Z. Wang, P. Yi, C. Chen, B. Huang, Y. Luo, J. Ma, and J. Jiang, “Multi-scale progressive fusion network for single image deraining,” in *Proc. IEEE CVPR*, pp. 8346–8355, 2020.